

A Machine Learning Model for Predicting the Shear Strength of Slender FRP-Reinforced Concrete Elements

Nermin M. Salem¹, Denise-Penelope N. Kontoni^{2,3,*}, Ahmed Farouk Deifalla⁴ and Ambrosios-Antonios Savvides^{5,6}

¹Department of Electrical Engineering, Faculty of Engineering and Technology, Future University in Egypt, New Cairo 11835, Egypt

²Department of Civil Engineering, School of Engineering, University of the Peloponnese, GR-26334 Patras, Greece

³School of Science and Technology, Hellenic Open University, GR-26335 Patras, Greece

⁴Department of Structural Engineering and Construction Management, Faculty of Engineering and Technology, Future University in Egypt, New Cairo 11835, Egypt

⁵School of Civil Engineering, National Technical University of Athens, Zografou Campus, GR-15773 Athens, Greece

⁶Laboratory of Applied Mechanics, Department of Naval Science, Hellenic Naval Academy, 185 39 Piraeus, Greece

Received 30 August 2024; Accepted 29 January 2025

Abstract

One-way shear failure of Fiber-Reinforced Polymer-reinforced concrete (FRP-RC) elements occurs with no adequate warning as well as it happens in a complicated and devastating manner. Recent research efforts have yielded several pioneering works in this area; however, there is a lack of agreement on the physical understanding of the behavior continues to be an issue. Thus, in the current study, a Machine Learning shear strength model is developed for FRP-RC elements. A boosted regression model is developed and trained using an experimental database composed of 420 records. The boosted model has proved a better prediction accuracy using statistical measures, the model reported a variation coefficient (R^2) = 0.91, root mean square error (RMSE) = 13175 and mean absolute error (MAE) = 8.8684. Also, a study of the importance of the input parameters has been presented. The proposed model captured the depth effect, the wide beam effect, and the dowel action.

Keywords: Fiber-reinforced polymer (FRP), Slender FRP-reinforced concrete elements, One-way shear failure, Shear strength, Machine Learning, Boosted regression model.

1. Introduction

Revisiting the old problem, which is the shear design of reinforced concrete elements has been and continues to be a dilemma. This dilemma is influenced by various mechanisms and parameters; thus, no one model is capable of resolving it [1-4]. In addition, Fiber-Reinforced Polymer-Reinforced Concrete (FRP-RC) elements increase the uncertainty of this old problem by additional factors such as different Young's modulus for different FRP types, the linear behavior up to the failure of Fiber-Reinforced Polymer (FRP), etc. [5-7]. Thus, the demand for developing a robust model that is capable of capturing the behavior of FRP-RC elements under shear is growing [8-10]. This is crucial to attaining a greater comprehension of the shear failure and better shear provisions; thus, achieving the following: optimum material usage, reliable design, and life span [11-12].

For eight decades, researchers have attempted to develop shear strength physical models for steel reinforced concrete (RC) elements; thus, many models have been developed. Back in the 50s, simplified empirical models were the only option [13], which included the basic parameters considered significant for the shear strength [14]. In addition, other parameters were found to be significant, including the depth effect; this, future models included [15-17]. Moreover, the effect of the element shear slenderness, the fracture energy, and the maximum nominal aggregate depth [13, 18-19] were investigated and included in the modeling. Experimental

databases were used to calibrate these empirical models; however, the mechanism and true behavior were too ambiguous and complicated to model. Last but not least, advanced experimental measurements and numerical analysis techniques were implemented in recent studies to further explore the mechanism and true behavior under shear [20-22]. Therefore, a handful of mechanical models were developed based on a more advanced understanding of the contribution of each shear mechanism [23-25].

A handful of one-way shear models were developed for steel-RC elements, including the Critical Shear Crack theory, the compression chord, the compression field, the multi-action model, the crack sliding shear, the critical shear displacement, the Reineck, and the Shear Crack Propagation [21, 26-35]. However, very limited models focused on FRP-reinforced concrete elements under shear. Those models include the compression chord, field, and Modified compression field models [36-39].

Artificial Intelligence (AI) has recently been increasingly used in various applications due to computing innovations. Machine Learning (ML) is a subset of AI trained and tested using large databases, increasing the prediction accuracy. ML techniques have become a powerful alternative for establishing an accurate prediction model based on experimental data. Many ML approaches have been used in the prediction of shear strength, such as artificial neural networks (ANN), multiple linear regression (MLR), support vector machine (SVM), and ensemble boosted regression. ANN and SVM are considered traditional ML techniques. These techniques

have distinct frameworks with strong and weak aspects; therefore, these algorithms still need further tuning. Ensemble techniques were proposed to benefit from the many abilities of each individual model.

Machine learning (ML) methods have been extensively utilized in concrete research, enabling comprehensive and in-depth studies within this field; the scalability and adaptability of boosted machine learning algorithms make them highly suitable for broader applications. It is designed to handle large and complex datasets efficiently, leveraging parallelization techniques to process high-dimensional data, ensuring scalability for real-world scenarios. Additionally, their inherent flexibility allows adaptation to various problem domains by retraining with new datasets or updating hyperparameters, making them applicable to diverse applications such as predicting shear strength for different FRP materials, structural configurations, or environmental conditions. Furthermore, feature importance analysis in boosted models offers valuable insights into critical parameters, enabling domain-specific customization and improved decision-making. Highlighting these attributes confirms the algorithm's potential for practical deployment in diverse engineering problems, enhancing the study's relevance and significance [40-52].

In this research, one of the most precise ensemble algorithms, the boosting ensemble regression model, is adapted to simulate the slender FRP-reinforced concrete elements. It is considered a powerful ML based on the employment of various weak learners to decrease overfitting, and it also shows superior prediction results when compared with any other ML models [40]. The model was trained with an experimental database composed of 420 samples. The final results proved that the boosted model exhibits the most robust and accurate predictions for the shear strength.

2. Experimental Database

The most thorough database for slender FRP-RC beams accessible to date, which consists of 420 specimens tested in 57 studies, is adopted in the present study [1, 2]. Table 1 and Figure 1 show the frequency distribution of the geometrical and mechanical parameters of the database. The database specimens have FRP flexure reinforcement, including, and not limited to, two Aramid-FRP (AFRP) bars, nine Basalt-FRP (BFRP) bars, 111 Carbon-FRP (CFRP) bars, and 298 Glass-FRP (GFRP) bars. The element width (b) ranges between 89 mm and 1830 mm, the effective depth (d) ranges between 73 mm and 938 mm, the compressive strength of concrete (f_c') range between 20 MPa and 93 MPa, the flexural reinforcement ratio (ρ_f) range between 0.09% and 3.98%, the young's modulus (E_f) value between 29 and 192 GPa, and the rupture stress of the FRP (f_{fu}) value between 397 and 2640 MPa.

Table 1. Distribution of parameters for database.

Source	Range
Size of the database	420
Studies in the database	57
Compressive strength of concrete (f_c' , MPa)	20 – 93
Element width (b, mm)	89 – 1830
Element effective depth (d, mm)	73 – 938
Shear span (a, mm)	299.6 – 3096
Shear span to depth ratio (a/d)	2.5 – 16.2
Ratio of longitudinal reinforcement ρ_f (%)	0.09 – 3.98
Young's modulus ratio of longitudinal reinforcement (E_f , GPa)	29 – 192

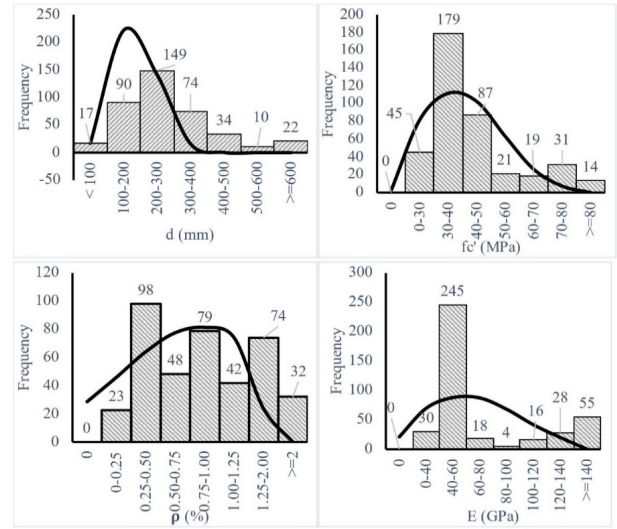


Fig. 1. Database frequency distribution.

3. Development and Validation of the Machine Learning (ML) Model

The boosted ensemble regression method is a statistical methodology used in developing a strong, accurate prediction model. It has also improved traditional decision tree methods. It creates several weak models to produce an optimal single model to reduce overfitting [40], which allows this method to work on different datasets and maintain the same efficient, accurate results.

For a given dataset with n records and p input features $D = \{X_i, y_i\}$, The output prediction is defined by:

$$Y_i = \sum_{i=1}^I f_i(X_i), f_i \in F \quad (1)$$

where, F is the regression tree space.

$$F = \{f(X) = w_{p(x)}\} \quad (2)$$

where, I is the number of trees. Each f_i is corresponding to p , an independent tree structure, and w leaf weights. The objective function is expressed by:

$$\text{Loss} = \sum_i L(Y_i, y_i) + \sum_i \varphi(f_i) \quad (3)$$

The prediction of the k^{th} instance at the n^{th} iteration is defined by:

$$Y_k^{(n)} = Y_k^{(n-1)} + f_i(X_i) \quad (4)$$

Also, the objective function could be updated as in:

$$\text{Loss}^{(n)} = \sum_{k=1}^I \text{Loss}(y_i, Y_k^{(n-1)} + f_i(X_i) + \varphi(f_i)) \quad (5)$$

where

$$\varphi(f_i) = \gamma T + \frac{1}{2} \lambda \sum_{j=1}^T w_j^2 \quad (6)$$

The boosted method employs second-order Taylor optimization for optimizing the objective function:

$$\text{Loss}^{(n)} \cong \sum_{k=1}^I [\text{Loss}(y_i, Y_k^{(n-1)} + g_i f_i(X_i) + \frac{1}{2} h_i f_i^2(X_i)) + \varphi(f_i)] \quad (7)$$

where, $g_i = \frac{\delta Loss(y_i, Y_k^{(n-1)})}{\delta Y_k^{(n-1)}}$ and $h_i = \frac{\delta^2 L(y_i, Y_i^{k-1})}{\delta Y_k^{(n-1)}}$

The final objective function is defined as follows:

$$Loss^{(n)}(p) = -\frac{1}{2} \sum_{j=1}^T \frac{(\sum_{i \in I_j} g_i)^2}{h_i + \lambda} + \gamma T \tag{8}$$

Figure 2 shows a flowchart of how the Boosted Algorithm works. For best output results, 15-fold held-out validation is used and applied to the model. The model is trained using the experimental dataset composed of six input features as previously defined in previous sections. This dataset was divided into two main sets; the training set contains 70% of the dataset records, and the testing set contains the remaining 30%. The number of trees used in the training process was set to 100 with a learning rate equal to 0.1. The needed reduction in the minimum loss for further partitioning each tree leaf node is set to 0. The model was implemented using MATLAB.

Figure 3 compares the experimentally real results and the predictions produced during the training phase. The model can accurately predict the shear strength with a higher accuracy than other constitutive models.

Figure 4 shows the prediction performance of the boosted model, where the x-axis represents the experimental test data while the y-axis represents the produced predicted output, respectively. The ideal predictions are represented by the black straight line, where the predictions are equal to the real output, while the predictions are presented by the pink dots. The vertical difference between the black line and the pink dots is the error in predictions. Most of the predicted points are located beneath the black diagonal line. This could also be used as a safety margin during the design process. However, it does not influence the analysis process.

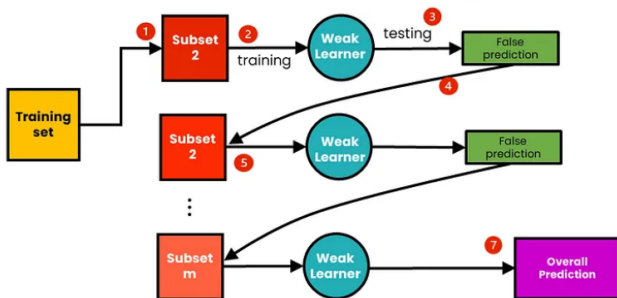


Fig. 2. Flow Chart of the boosted Algorithm.

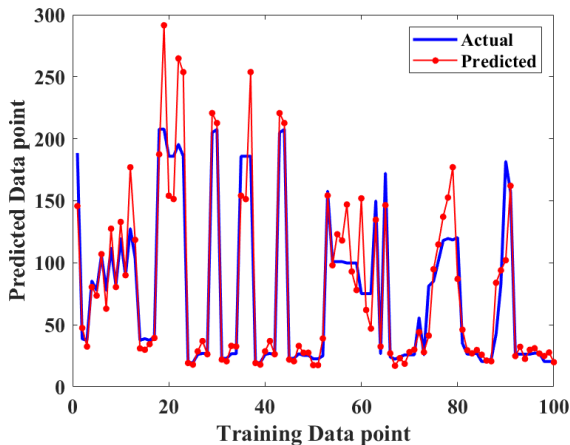


Fig. 3. Predicted versus Actual data points during the Training Phase.

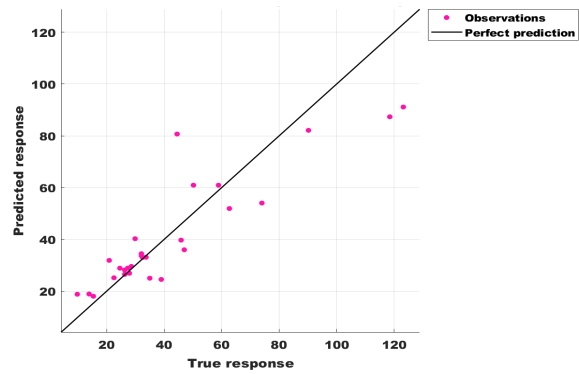


Fig. 4. Prediction results of the boosted model for the testing dataset.

Performance evaluation was performed by computing some common statistical measures such as the variation coefficient (R^2), root mean square error (RMSE), and mean absolute error (MAE). The performance metrics considered have been carefully chosen and implemented to assure the accuracy of the proposed model over existing ones. Thus, the proposed model provides reliable and more accurate predictions of the shear capacity of the non-slender FRP-reinforced beams, ultimately leading to a safer and more economically resilient structure. R^2 reports how well the proposed model can predict the trained data. RMSE is the cost function that plays a fundamental role in the learning process of the boosted model. RMSE and MAE play a vital role in the accuracy of the predictions that are obtained. The boosted model reported $R^2 = 0.91$, RMSE = 13175 and MAE = 8.8684. The training loss is shown in Figure 5.

Figure 6 provides a study of the importance of the six input parameters. That study concluded that the dominant parameters are the d, followed by the element width-to-depth ratio, thus emphasizing the importance of the depth and the wide beam effect (i.e., rectangularity ratio). Therefore, potential biases, such as overrepresenting certain FRP types (e.g., Glass-FRP), won't influence the model performance as Ef has minimal effect on the FRP-shear strength.

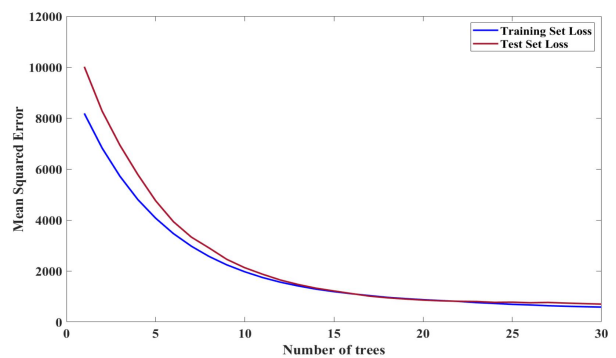


Fig. 5. Training Loss.

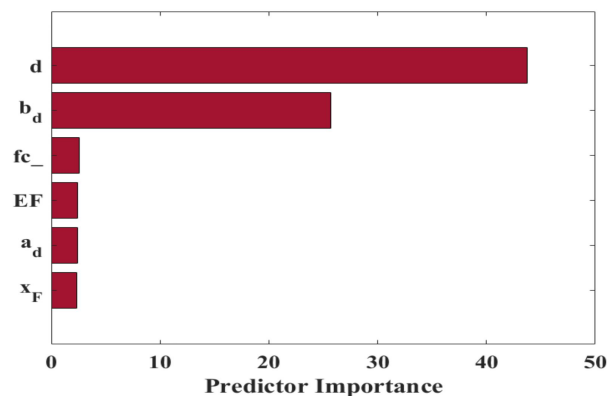


Fig. 6. Importance of the six input parameters.

4. Comparison between Selected Models and the Proposed Model

Several methods for concrete elements under shear with FRP reinforcements have been developed, and a handful of these

models, namely the selected models M, DN, and B, were selected and implemented as shown in Table 2 to be compared to the proposed ML model.

Table 2. The selected methods.

Method	Shear resistance, V	Symbols
M [36]	The compression chord model: $\xi \left[(1.072 - 0.01n) \frac{c}{d} + 0.036 \right] f_{ct} bd$	$\xi = 1.2 - 0.2 \frac{a}{d}$ $\frac{c}{d} = n\rho \left(-1 + \sqrt{1 + \frac{2}{n\rho}} \right)$
DN [37]	The compression field-based model: $AE \left(\frac{-2.58 + \sqrt{7.18 + \frac{10506(0.15l_b + 0.72c)bf'_c}{AE}}}{5253} \right)$	$V \geq 0.14(0.15l_b + 0.72c)bf'_c$
B [38]	Based on the MCFT [39], the following model was developed: $0.07 \left(\frac{E_p b}{f'_c d} \right) \sqrt{f'_c} bd$	$0.05\sqrt{f'_c} bd \leq V \leq 0.3\sqrt{f'_c} bd$

4.1 Overview

Figure 7 depicts the measured versus the calculated strength employing the ML, B, M and DN methods, respectively, as well as for each of them, the theoretical line representing the best-fit line, an ideal 45 degrees line, and the χ factor. The χ factor, derived as the inverse of the slope of the trend line, serves as an indicator of the under- or over-estimation of the employed method. Also, Table 3 displays the variation of the SR, which is the ratio between the measured and the calculated strength employing different methods. The statistical measures include the maximum, the minimum, the average, the variation coefficient, and the median. The ML showed excellent accuracy with a χ value of 1.12 and an average SR value of 1.01. With a factor χ value of 0.42 and an average SR value of 0.46, the B model is the least conservative. While, for the other models, the χ factor ranged between 0.65-0.91 and the average SR value ranged between 0.47-0.96. With respect to consistency, the variation coefficient ranged between 42% to 53%, indicating a significant lack of consistency. While the proposed ML model showed excellent consistency with a variation coefficient value of 21%. With respect to safety, the ML and M models showed a lower 95% of values above 0.85, which is reasonably safe. Still, the B and DN models showed a lower 95% value than 0.85, which needs further improvement for the design purpose. The correlation coefficient between the measured and the calculated strength for the ML, B, M and DN methods showed a value of 0.95, 0.88, 0.86 and 0.66, respectively. Although calculated strength for all methods was found to be in correlation to that experimentally measured; however, the DN was the weakest correlation. Finally, the strength calculated using the ML model is the most accurate, the most consistent, and the strongest in correlation compared to the measured strength.

Table 3. Statistical measures for the SR.

	M	DN	B	ML
Mean	0.96	0.65	0.47	1.01
C.O.V. (Coefficient of Variation)	46%	63%	48%	21%
L.L. 99% (Lower Limit 99%)	0.91	0.60	0.44	0.98
Minimum	0.31	0.09	0.13	0.47
Maximum	3.04	2.68	1.68	2.02
Median	0.82	0.61	0.40	1.00
Correlation coefficient	0.87	0.68	0.88	0.95

4.2 Effect of Size

Table 4 demonstrates the correlation coefficient between SR versus element size. For ML, M, DN and B models, the coefficient of correlation between depth and the SR was 0.08, 0.43, 0.86 and 0.13, respectively. Thus, the ML and B models' predictions are weakly correlated to the depth compared to the DN and M models. Moreover, Figure 8 exhibits the calculated SR for ML, M, DN, and B models plotted against depth, along with the corresponding best-fit line for each model. Moreover, the slope of the trend line for the Calculated SR for ML, M, DN and B models versus the depth are values of 0.0001, 0.001, 0.002 and 0.0002, respectively. Safety decreases as depth decreases across all models consistently. The M and DN are less consistent versus depth compared to other models. The proposed ML model is more consistent and well-presented versus depth compared to other models.

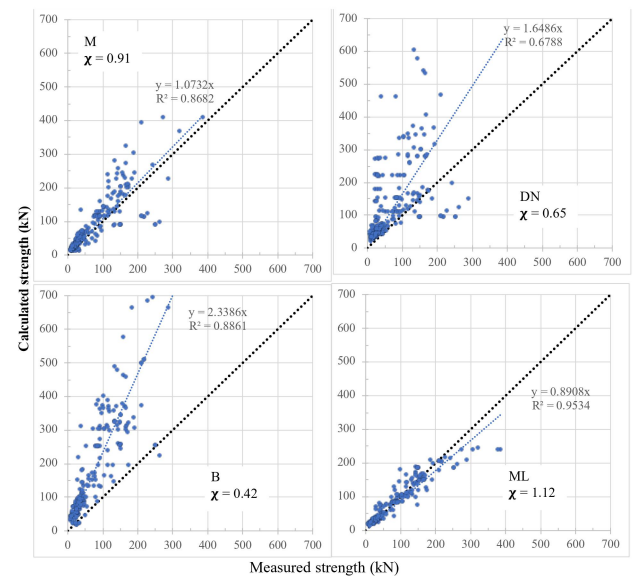


Fig. 7. Calculated versus measured strength for selected (M, DN, B and ML) models.

4.3 Effect of Compressive Strength of Concrete

The coefficient of correlation between the compressive strength of concrete and the calculated SR using ML, B, M and DN, was found to be -0.00, -0.12, -0.17 and -0.41,

respectively, as per Table 4. Therefore, the calculated SR using all methods, except the DN, is weakly correlated to the compressive strength of concrete. Furthermore, Figure 9 illustrates the calculated SR using ML, M, DN and B models plotted against the compressive strength of concrete, along with the corresponding best-fit-line for each model. Moreover, the slope of the trend line for the calculated SR for ML, B, M and DN models versus the compressive strength of concrete are values of 0.00002, -0.0017, -0.0047 and -0.0103, respectively. Except for the ML model, the safety of models decreases with the increase in the compressive strength of concrete. DN is the least consistent with respect to the compressive strength of concrete compared to other models. Thus, it needs further investigation into the compressive strength of concrete. The proposed ML model is more consistent and well-presented versus the compressive strength of concrete compared to other methods.

Table 4. Coefficient of correlation between variables and models.

	M	DN	B	ML
Size	0.43	0.86	0.13	0.08
Compressive strength of concrete	-0.17	-0.41	-0.12	0.00
Ratio of longitudinal reinforcement	-0.44	-0.12	-0.09	0.08
FRP Young's modulus	-0.23	0.02	0.08	0.07

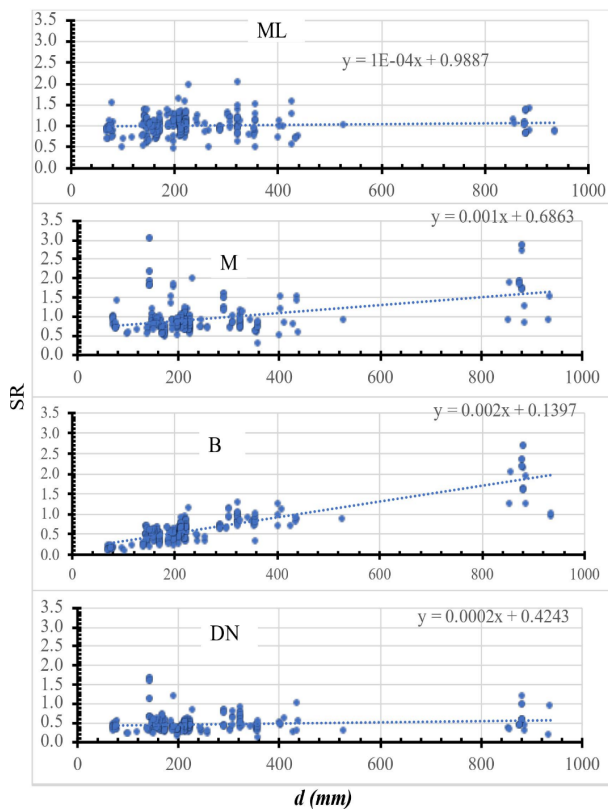


Fig. 8. Calculated SR using selected models (ML, M, B and DN) versus size.

4.4 Effect of Reinforcement Young's Modulus

From Table 4, the coefficient of correlation between reinforcement Young's modulus and calculated SR using ML, M, DN and B was 0.07, -0.23, 0.02 and 0.08, respectively. Therefore, the calculated SR using M methods is highly correlated to the reinforcement ratio compared to other models (Figure 10); thus, it needs further investigation into the reinforcement Young's modulus. Additionally, Figure 11 presents the calculated SR using ML, M, DN and B models versus the reinforcements Young's modulus, along with the best-fit-line for each

model. Moreover, the slope of the trend line for the calculated SR using ML, M, DN and B methods versus the reinforcement Young's modulus are the values of 0.0004, -0.0026, 0.0002 and 0.0005, respectively. Except for the M model, the safety decreases with the increase in the flexure reinforcement Young's modulus for all models. The ML is more consistent with Flexure reinforcement Young's modulus compared to other models. The proposed ML model is more consistent and well-presented versus FRP Young's modulus compared to other models. Boosted ML algorithms consistently outperform traditional methods as shear strength models must account for the variability in material properties, environmental conditions, and testing methods. Traditional models are often based on rigid assumptions that limit their applicability outside predefined conditions. Boosted ensemble methods excel because:

- They are data-driven, relying on the richness of the dataset rather than predefined equations.
- They are adaptive, adjusting for different scales, conditions, and data distributions.
- They provide explainability, such as feature importance, helping users understand the key factors influencing predictions.

Therefore, the ML model's ability to capture intricate, high-dimensional relationships and adapt to new data without explicit assumptions makes it a more versatile and robust tool than traditional models.

Last but not least, implementing this accurate and reliable proposed model in the design of new structures will guarantee optimized material and factor of safety. Thus, the cost savings are tremendous, opening the door for a new era of resilient structures with maximum potential and minimal probability of failure.

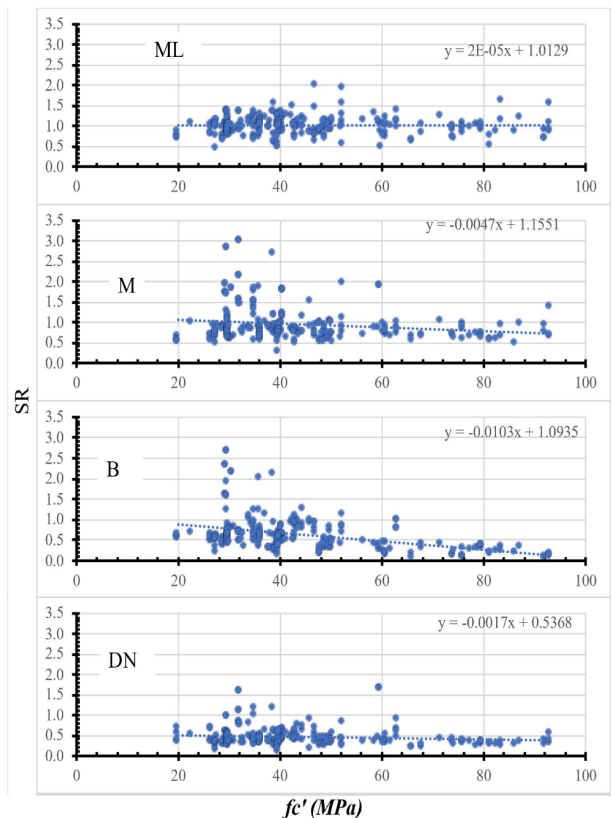


Fig. 9. Calculated SR utilizing selected models (ML, M, B and DN) versus compressive strength of concrete.

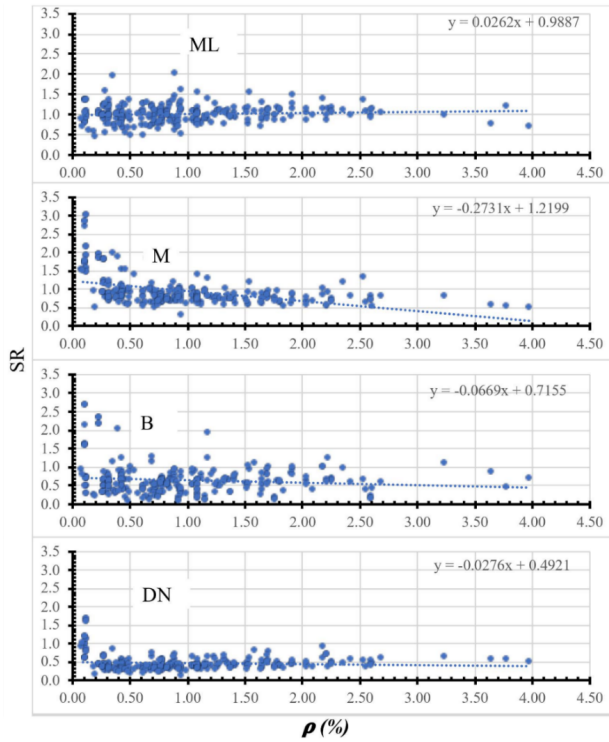


Fig. 10. Calculated SR utilizing selected models (ML, M, B and DN) versus the flexure reinforcement's ratio.

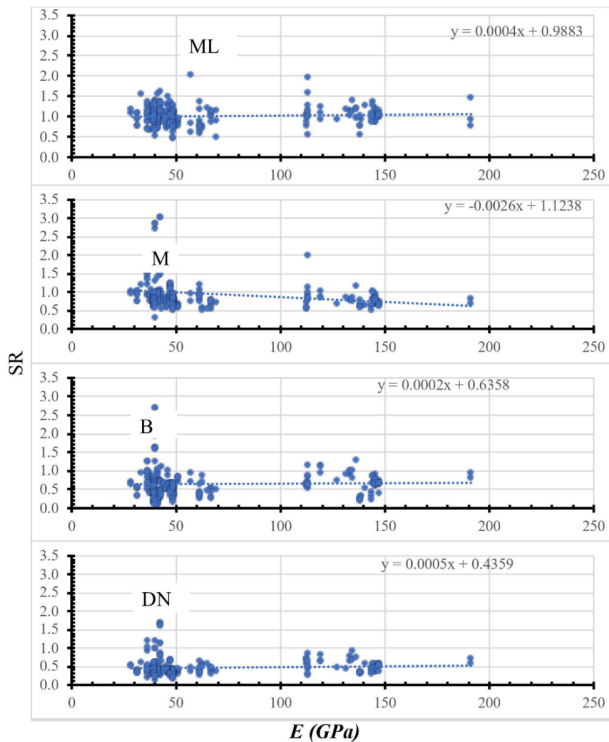


Fig. 11. Calculated SR utilizing selected models (ML, M, B and DN) versus the flexure reinforcement Young's modulus.

5. Parametric Study

In order to further examine the potential of the proposed model, a case study was implemented where Figure 12 shows behavior trends of the strength versus the effective depth, width-to-depth ratio, compressive strength of concrete, ratio

of longitudinal reinforcement, and flexure reinforcement Young's modulus. For the effective depth, the predicted behavior shows two-fold as follows: (1) large strength for elements depth of less than 200 mm; (2) a steady decrease of the strength with depth for elements with a depth of more than 200 mm. The model captured the depth effect.

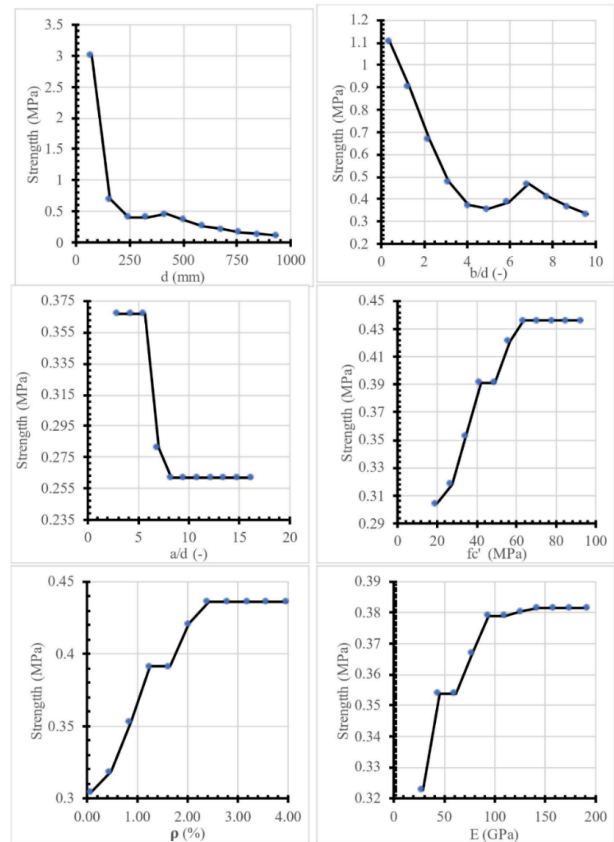


Fig. 12. Behavior trends observed using the proposed model.

For the element width-to-depth ratio, the behavior trend is two folds as follows: (1) highly nonlinear for a width-to-depth ratio less than 7, where the strength decreases with the increase in the width-to-depth ratio; (2) a linear decrease in the strength for ratio between 7 to 9. The mode captures the effect of the wide beam.

For the shear slenderness ratio, the observed behavior is in three folds as follows: (1) almost constant from a value of 3 to 5; (2) a linear decrease up to the value of 8; (3) almost constant up to the value of 16. The proposed model captured the failure model, where elements with a high shear slenderness ratio fail mainly due to flexure.

For the compressive strength of concrete, the observed behavior is into three folds as follows: (1) a linear increase up to the value of 40 MPa; (2) a linear increase from compressive strength of concrete from the value of 40 to 60 MPa; (3) almost constant for value more than 60 MPa. The model captured the difference in behavior between the normal strength of the concrete, the high-strength concrete, and the ultra-high strength concrete.

For the ratio of longitudinal reinforcement, the observed behavior is into three folds as follows: (1) a nonlinear increase up to 1%; (2) a linear increase from a value of 1% up to the value of 2.5%; (3) an almost constant up to the value of 4%. The model captured the dowel effect, which is dependent on the value of the ratio of longitudinal reinforcement.

For the flexure reinforcement Young's modulus, the observed behavior is into three folds as follows: (1) a linear increase from 40 GPa to 50 GPa; (2) a linear increase from the value of 50 GPa up to the value of 100 GPa; (3) almost constant for Young's modulus more than 100 GPa. The proposed model showed an interesting behavior. Also, the model is primarily developed and validated based on the provided data range, including slender beams. While the methodology and underlying principles could be extended to other configurations, its direct applicability to non-slender beams or significantly different configurations would require additional validation and potentially new data.

6. Future recommendations

The boosted ML model has demonstrated high effectiveness within the data range on which it was trained. However, its performance may be limited when applied to scenarios beyond this range, such as non-slender beams or significantly different configurations. This limitation stems from its reliance on the training data, which directly influences its generalization ability.

To further validate the robustness and generalizability of the proposed machine learning shear strength model, future studies should focus on testing the model using additional datasets. This includes incorporating independent datasets from diverse experimental programs or real-world case studies to evaluate its performance under varied conditions. Furthermore, applying the model to the design of real-world FRP-RC elements subjected to actual load conditions would provide valuable insights into its practical applicability and reliability in field settings. Expanding these evaluations would help to understand the model's limitations better and enhance its utility across a broader range of structural applications.

Additionally, the model's interpretability can be challenging due to the complex nature of boosted algorithms. While it provides accurate predictions, understanding the underlying physical behavior might require supplementary analysis.

7. Conclusions

Using an experimental database for FRP-reinforced concrete beams failing in shear with a total of 420 records, a machine

learning (ML) boosted regression model for shear of slender FRP-reinforced concrete beams was developed, validated, and implemented in a parametric study; thus, the following concluding remarks were reached as follows:

- The proposed model captured the effect of (1) the beam depth; (2) the wide beam; (3) the failure model, where elements with a high shear slenderness ratio fail mainly due to flexure; (4) the difference between the normal strength of the concrete, the high strength concrete, and the ultrahigh strength concrete; (5) the dowel effect, which is dependent on the value of the ratio of longitudinal reinforcement; (6) different strength patterns depending on the value of Young's modulus.
- The boosted model has proved a better prediction accuracy using statistical measures, whereas the model reported a variation coefficient (R^2) = 0.91, a root mean square error (RMSE) of 13175 and a mean absolute error (MAE) of 8.8684.
- The importance of the variables is effective beam depth, width-to-depth ratio, concrete compressive strength, FRP Young's modulus, shear span, and FRP percentage, respectively. Thus, the effective depth of the beam and the width-to-depth ratio are the most critical factors.

Future studies would be:

- Develop models for non-slender FRP-reinforced concrete beams.
- Develop design guidelines for slender and non-slender FRP-reinforced concrete beams.
- Develop mechanical models for slender and non-slender FRP-reinforced concrete beams.
- Investigate the machine learning models, design guidelines and mechanical models for punching shear of FRP-reinforced concrete slabs.

This is an Open Access article distributed under the terms of the Creative Commons Attribution License.



References

- [1] A. H. Ali, M. Hamady, C. E. Chalioris, and A. Deifalla, "Evaluation of the shear design equations of FRP-reinforced concrete beams without shear reinforcement," *Eng. Struct.*, vol. 235, May 2021, Art. no. 112017, doi: 10.1016/j.engstruct.2021.112017.
- [2] N. M. Salem and A. Deifalla, "Evaluation of the strength of slab-column connections with FRPs using machine learning algorithms," *Polym.*, vol. 14, Apr. 2022, Art. no. 1517, doi: 10.3390/polym14081517.
- [3] S. Alkhatib and A. Deifalla, "Punching shear strength of FRP-reinforced concrete slabs without shear reinforcements: A reliability assessment," *Polym.*, vol. 14, Apr. 2022, Art. no. 1743, doi: 10.3390/polym14091743.
- [4] A. Deifalla and N. M. Salem, "A machine learning model for torsion strength of externally bonded FRP-reinforced concrete beams," *Polym.*, vol. 14, Apr. 2022, Art. no. 1824, doi: 10.3390/polym14091824.
- [5] A. Deifalla, "Punching shear strength and deformation for FRP-reinforced concrete slabs without shear reinforcements," *Case Stud. Constr. Mater.*, vol. 16, Jun. 2022, Art. no. e00925, doi: 10.1016/j.cscm.2022.e00925.
- [6] A. Deifalla, "Refining the torsion design of fibered concrete beams reinforced with FRP using multivariable non-linear regression analysis for experimental results," *Eng. Struct.*, vol. 226, Jan. 2021, Art. no. 111394, doi: 10.1016/j.engstruct.2020.111394.
- [7] A. Deifalla, "Torsion design of lightweight concrete beams without or with fibers: A comparative study and a refined cracking torque formula," *Struct.*, vol. 28, pp. 786–802, Dec. 2020, doi: 10.1016/j.istruc.2020.09.004.
- [8] M. M. Hassan and A. Deifalla, "Evaluating the new CAN/CSA-S806-12 torsion provisions for concrete beams with FRP reinforcements," *Mater. Struct.*, vol. 49, pp. 2715–2729, Jul. 2015, doi: 10.1617/s11527-015-0680-9.
- [9] A. Deifalla, "Torsional behavior of rectangular and flanged concrete beams with FRP," *J. Struct. Eng. (ASCE)*, vol. 141, no. 12, May 2015, doi: 10.1061/(ASCE)ST.1943-541X.0001322.
- [10] A. Deifalla, M. S. Khali, and A. Abdelrahman, "Simplified model for the torsional strength of concrete beams with GFRP stirrups," *J. Compos. Constr. (ASCE)*, vol. 19, no. 1, Jun. 2015, doi: 10.1061/(ASCE)CC.1943-5614.0000498.

- [11] A. Deifalla, "Strength and ductility of lightweight reinforced concrete slabs under punching shear," *Struct.*, vol. 27, pp. 2329–2345, Oct. 2020, doi: 10.1016/j.istruc.2020.08.002.
- [12] A. Deifalla and A. Ghobarah, "Full torsional behavior of RC beams wrapped with FRP: Analytical model," *J. Compos. Constr. (ASCE)*, vol. 14, no. 3, Feb. 2010, doi: 10.1061/(ASCE)CC.1943-5614.0000085.
- [13] T. C. Zsutty, "Beam shear strength prediction by analysis of existing data," *ACI J. Proc.*, vol. 65, no. 11, pp. 943–951, Jan. 1968, doi: 10.14359/7526.
- [14] F. Leonhardt, R. Walther, and W. Dilger, "Schubversuche an Durchlaufträger (Zweifeldrige Stahlbetonbalken mit und ohne Schubbe-wehrung): DAfStb-Heft 163," Ernst & Sohn, Berlin, Germany, 1964.
- [15] O. Hedman and A. Losberg, *Design of Concrete Structures with Regard to Shear Forces, in Shear and Torsion: Explanatory and View-point Papers on Model Code, Chapters 11 and 12*, P. E. Regan and H. P. J. Taylor, Eds. Lausanne, Switzerland: International Federation for Structural Concrete, 1978, pp. 184–209.
- [16] Z. P. Bazant and J.-K. Kim, "Size effect in shear failure of longitudinally reinforced beams," *ACI J. Am. Concr. Inst.*, vol. 81, no. 5, pp. 456–468, Sep. - Oct. 1984.
- [17] W. M. Ghannoum, "Depth effect on shear strength of reinforced concrete beams," M.S. Thesis, McGill Univ., Montreal, QC, Canada, Nov. 1998.
- [18] E. C. Bentz, "Empirical modeling of reinforced concrete shear strength depth effect for members without stirrups," *ACI Struct. J.*, vol. 102, pp. 232–241, Mar. 2005.
- [19] Z. P. Bazant and J. Planas, *Fracture and Depth Effect in Concrete and Other Quasi-Brittle Materials*. Boca Raton, FL, USA: CRC Press, 1998.
- [20] A. Muttoni and M. Fernández Ruiz, "Shear strength of members without transverse reinforcement as a function of critical shear crack width," *ACI Struct. J.*, vol. 105, pp. 163–172, Mar. 2008.
- [21] F. J. Vecchio and M. P. Collins, "The modified compression-field theory for reinforced concrete elements subjected to shear," *ACI Struct. J.*, vol. 83, pp. 219–231, Jan. 1986, doi: 10.14359/10416.
- [22] N. D. Tung and N. V. Tue, "A new approach to shear design of slender reinforced concrete members without transverse reinforcement," *Eng. Struct.*, vol. 107, pp. 180–194, Jan. 2016, doi: 10.1016/j.engstruct.2015.04.015.
- [23] P. Huber, T. Huber, and J. Kollegger, "Investigation of the shear behavior of RC beams on the basis of measured crack kinematics," *Eng. Struct.*, vol. 113, pp. 41–58, Apr. 2016, doi: 10.1016/j.engstruct.2016.01.025.
- [24] F. Cavagnis, "Shear in reinforced concrete without transverse reinforcement: From refined experimental measurements to mechanical models," Ph.D. Thesis, École Polytechnique Fédérale de Lausanne, Lausanne, Switzerland, Dec. 2017.
- [25] A. Cladera, A. Mari, J.-M. Bairán, E. Oller, and C. Ribas, "One-way shear design method based on a multi-action model: A compromise between simplicity and accuracy," *ACI Concr. Int.*, vol. 39, no. 9, pp. 40–46, Sep. 2017.
- [26] M. Zink, "Zum Biegeschubversagen schlanker Bauteile aus Hochleistungs-beton mit und ohne Vorspannung," Ph.D. Thesis, Universität Leipzig, Leipzig, Germany, Jan. 1999.
- [27] P. D. Zararis and G. C. Papadakis, "Diagonal shear failure and depth effect in RC beams without web reinforcement," *J. Struct. Eng.*, vol. 127, pp. 733–742, Jul. 2001, doi: 10.1061/(ASCE)0733-9445(2001)127:7(733).
- [28] E. C. Bentz, F. J. Vecchio, and M. P. Collins, "Simplified modified compression field theory for calculating shear strength of reinforced concrete members," *ACI Struct. J.*, vol. 103, pp. 614–624, Jan. 2006, doi: 10.14359/16438.
- [29] Y. Yang, "Shear behaviour of reinforced concrete members without shear reinforcement: A new look at an old problem," Ph.D. Thesis, Delft University of Technology, Delft, The Netherlands, Apr. 2014.
- [30] Y. Yang, J. Walraven, and J. D. Uijl, "Shear behavior of reinforced concrete beams without transverse reinforcement based on critical shear displacement," *J. Struct. Eng.*, vol. 143, no. 1, Jul. 2017, doi: 10.1061/(ASCE)ST.1943-541X.0001608.
- [31] J. Fisker and L. G. Hagsten, "Mechanical model for the shear capacity of R/C beams without stirrups: A proposal based on limit analysis," *Eng. Struct.*, vol. 115, pp. 220–231, May 2016, doi: 10.1016/j.engstruct.2016.02.035.
- [32] N. V. Tue, W. Theiler, and N. D. Tung, "Schubverhalten von Biegebauteilen ohne Querkraftbewehrung," *Beton-Stahlbetonb.*, vol. 109, pp. 666–677, Oct. 2014, doi: 10.1002/best.201400058.
- [33] A. Muttoni and M. Fernández Ruiz, "From experimental evidence to mechanical modeling and design expressions: The Critical Shear Crack Theory for shear design," *Struct. Concr.*, vol. 20, pp. 1464–1480, Jun. 2019, doi: 10.1002/suco.201900193.
- [34] K.-H. Reineck, "Ultimate shear force of structural concrete members without transverse reinforcement derived from a mechanical model," *ACI Struct. J.*, vol. 88, pp. 592–602, Sep. 1991.
- [35] M. Classen, "Shear Crack Propagation Theory (SCPT) – The mechanical solution to the riddle of shear in RC members without shear reinforcement," *Eng. Struct.*, vol. 210, May 2020, Art. no. 110207, doi: 10.1016/j.engstruct.2020.110207.
- [36] A. Mari, A. Cladera, E. Oller, and J. Bairán, "Shear design of FRP reinforced concrete beams without transverse reinforcement," *Compos. Part B: Eng.*, vol. 57, pp. 228–241, Feb. 2014, doi: 10.1016/j.compositesb.2013.10.005.
- [37] K. Dhahir and W. Nadir, "A compression field-based model to assess the shear strength of concrete beams reinforced with longitudinal FRP bars," *Constr. Build. Mater.*, vol. 191, pp. 736–751, Dec. 2018, doi: 10.1016/j.conbuildmat.2018.10.036.
- [38] H. Baghi, J. A. Barros, M. Kaszubska, and R. Kotynia, "Shear behavior of concrete beams reinforced exclusively with longitudinal glass fiber reinforced polymer bars: Analytical model," *Struct. Concr.*, vol. 19, no. 1, pp. 162–173, Mar. 2018, doi: 10.1002/suco.201700175.
- [39] E. C. Bentz, L. Massam, and M. P. Collins, "Shear strength of large concrete members with FRP reinforcement," *J. Compos. Constr. (ASCE)*, vol. 14, no. 6, pp. 637–646, Feb. 2010, doi: 10.1061/(ASCE)CC.1943-5614.0000108.
- [40] N. M. Salem and A. Deifalla, "Evaluation of the strength of slab-column connections with FRPs using machine learning algorithms," *Polym.*, vol. 14, no. 8, Apr. 2022, Art. no. 1517, doi: 10.3390/polym14081517.
- [41] M. Liang, Z. Chang, Z. Wan, Y. Gan, E. Schlangen, and B. Šavija, "Interpretable ensemble-machine-learning models for predicting creep behavior of concrete," *Cem. Concr. Compos.*, vol. 125, Jan. 2022, Art. no. 104295, doi: 10.1016/j.cemconcomp.2021.104295.
- [42] N. Badra, S. Haggag, A. Deifalla, and N. M. Salem, "Development of machine learning models for reliable prediction of the punching shear strength of FRP-reinforced concrete slabs without shear reinforcements," *Meas.*, vol. 201, Sep. 2022, Art. no. 111723, doi: 10.1016/j.measurement.2022.111723.
- [43] H. C. Arora, S. Kumar, D.-P. N. Kontoni, A. Kumar, M. Sharma, N. R. Kapoor, and K. Kumar, "Axial capacity of FRP-reinforced concrete columns: Computational intelligence-based prognosis for sustainable structures," *Buildings*, vol. 12, no. 12, Dec. 2022, Art. no. 2137, doi: 10.3390/buildings12122137.
- [44] H. Naderpour, M. Akbari, M. Mirrashid, and D.-P. N. Kontoni, "Compressive capacity prediction of stirrup-confined concrete columns using neuro-fuzzy system," *Buildings*, vol. 12, no. 9, Sep. 2022, Art. no. 1386, doi: 10.3390/buildings12091386.
- [45] K. C. Onyelowe, A. M. Ebid, A. Riofrio, A. Soleymani, H. Baykara, D.-P. N. Kontoni, H. A. Mahdi, and H. Jahangir, "Global warming potential-based life cycle assessment and optimization of the compressive strength of fly ash-silica fume concrete; environmental impact consideration," *Front. Built Environ.*, vol. 8, Oct. 2022, Art. no. 992552, doi: 10.3389/fbuil.2022.992552.
- [46] K. C. Onyelowe, A. M. Ebid, H. A. Mahdi, A. Riofrio, D. R. Eidgah-ee, H. Baykara, A. Soleymani, D.-P. N. Kontoni, J. Shakeri, and H. Jahangir, "Optimal compressive strength of RHA ultra-high-performance lightweight concrete (UHPLC) and its environmental performance using life cycle assessment," *Civ. Eng. J.*, vol. 8, no. 11, pp. 2391–2410, Nov. 2022, doi: 10.28991/CEJ-2022-08-11-03.
- [47] M. Mirrashid, H. Naderpour, D.-P. N. Kontoni, A. Jakubczyk-Galczyńska, R. Jankowski, and T. N. Nguyen, "Optimized computational intelligence model for estimating the flexural behavior of composite shear walls," *Buildings*, vol. 13, no. 9, Sep. 2023, Art. no. 2358, doi: 10.3390/buildings13092358.
- [48] K. C. Onyelowe, J. Jagan, D.-P. N. Kontoni, A. A. B. Moghal, I. C. Onuoha, R. Viswanathan, and D. K. Soni, "Utilization of GEP and ANN for predicting the net-zero compressive strength of fly ash concrete toward carbon neutrality infrastructure regime," *Int. J. Low-Carbon Technol.*, vol. 18, pp. 902–914, Aug. 2023, doi: 10.1093/ijlct/ctad081.
- [49] S. Sharma, H. C. Arora, A. Kumar, D.-P. N. Kontoni, N. R. Kapoor, K. Kumar, and A. Singh, "Computational intelligence-based structural health monitoring of corroded and eccentrically loaded reinforced concrete columns," *Shock and Vib.*, vol. Feb. 2023, 2023, Art. no. 9715120, doi: 10.1155/2023/9715120.
- [50] K. C. Onyelowe, D.-P. N. Kontoni, S. R. M. Pilla, S. Hanandeh, A. M. Ebid, M. R. Ghadikolae, and L. U. Stephen, "Runtime-based metaheuristic prediction of the compressive strength of net-zero

traditional concrete mixed with BFS, FA, SP considering multiple curing regimes," *Asian J. Civ. Eng.*, vol. 25, pp. 1241–1253, Feb. 2024, doi: 10.1007/s42107-023-00839-3.

[51] D.-P. N. Kontoni and M. Ahmadi, "Practical prediction of ultimate axial strain and peak axial stress of FRP-confined concrete using hybrid ANFIS-PSO models," in *Artificial Intelligence Applications for Sustainable Construction 2024*, M. L. Nehdi, H. C. Arora, K. Kumar, R. Damaševičius, and A. Kumar, Eds. Cambridge, MA, USA:

Woodhead Publishing, Elsevier, Jan. 2024, pp. 225–255, doi: 10.1016/B978-0-443-13191-2.00015-8.

[52] H. Naderpour, M. Abbasi, D.-P. N. Kontoni, M. Mirrashid, N. Ezami, and A.-A. Savvides, "Integrating image processing and machine learning for the non-destructive assessment of RC beams damage," *Buildings*, vol. 14, no. 1, Jan. 2024, Art. no. 214, doi: 10.3390/buildings14010214.

List of Symbols

D	The dataset for training and testing
X_i	Input Features
y_i	Output Feature
Y_i	Predicted Output
F	Regression tree space
f_i	The i th number of regression tree
I	Total number of regression trees
w	Leaf weights
$L(Y_i, y_i)$	The error between the predicted and actual output
$\varphi(f_i)$	Regularization Term
γ	Regularization Parameter
T	The number of iterations or the number of boosting steps
λ	Other regularization term
w_j^2	The squared weights over all boosting steps
g_i	The first-order derivative of the loss function with respect to the predicted value. It represents the gradient.
h_i	The second-order derivative (Hessian) of the loss function with respect to the predicted value.